THE JOURNAL OF PHYSICAL CHEMISTRY Letters

Letter

pubs.acs.org/JPCL

# Temperature-Dependent Polarization in Field-Effect Transport and Photovoltaic Measurements of Methylammonium Lead Iodide

John G. Labram,[†,§] Douglas H. Fabini,[‡,§] Erin E. Perry,[‡,§] Anna J. Lehner,[‡,§] Hengbin Wang,[§] Anne M. Glaudell,[‡] Guang Wu,[∥] Hayden Evans,[‡,§] David Buck,[⊥] Robert Cotta,[⊥] Luis Echegoyen,[⊥] Fred Wudl,[†,‡,§] Ram Seshadri,[†,‡,§] and Michael L. Chabinyc*[,†,‡,§]

[†]California NanoSystems Institute (CNSI), [‡]Materials Research Laboratory, [§]Mitsubishi Chemical - Center for Advanced Materials, and [∥]Department of Chemistry & Biochemistry, University of California Santa Barbara, Santa Barbara, California 93106, United States

[⊥]Department of Chemistry, University of Texas El Paso, El Paso, Texas 79968, United States

Supporting Information

**ABSTRACT:** While recent improvements in the reported peak power conversion efficiency (PCE) of hybrid organic−inorganic perovskite solar cells have been truly astonishing, there are many fundamental questions about the electronic behavior of these materials. Here we have studied a set of electronic devices employing methylammonium lead iodide ((MA)$PbI_3$) as the active material and conducted a series of temperature-dependent measurements. Field-effect transistor, capacitor, and photovoltaic cell measurements all reveal behavior consistent with substantial and strongly temperature-dependent polarization susceptibility in (MA)$PbI_3$ at temporal and spatial scales that significantly impact functional behavior. The relative PCE of (MA)$PbI_3$ photovoltaic cells is observed to reduce drastically with decreasing temperature, suggesting that such polarization effects could be a prerequisite for high-performance device operation.

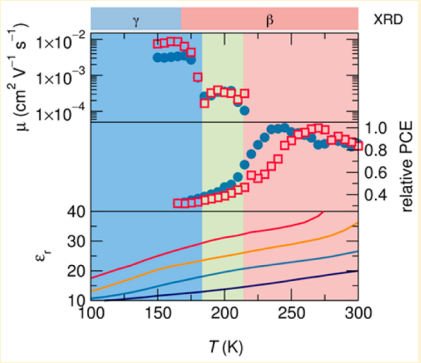


The pace at which new materials and designs for solar cells emerge is very slow,[1−6] and is arguably comparable to the discovery of high $T_c$ superconductors.[7,8] The finding that hybrid organic metal halide solar cells based on $CH_3NH_3PbI_3$ can lead to high power conversion efficiency (PCE) using simple coating methods, with a material comprising earth-abundant elements, has therefore garnered significant interest.[6,9,10] Not only has the peak reported PCE exceeded 20% in a short time,[11−13] but the processing techniques widely employed suggest that commercial products could be fabricated using low-cost, large-area techniques, compatible with flexible substrates.[14]

The $ABX_3$ perovskite crystal structure is characterized by a three-dimensionally corner-connected network of $BX_{6/2}$ octahedra that is filled by $A$ ions. Perovskite compounds where $A$ is an organic cation, $B$ is usually a main group element, and $X$ is a group 7 anion (halide) are referred to as hybrid organic−inorganic or hybrid-halide perovskites. Materials in this class are found to possess strong optical absorption,[6,15] impressive electrical properties[16] and an unusually low density of trap states,[17] resulting in the demonstration of solar cells with remarkably high PCEs.[6,9,11,13,14] In spite of the progress made in forming solar cells, there are many fundamental questions about the properties of the organic metal halide materials systems that enable this performance. Hybrid organic−inorganic perovskite solar-cells are notable for their various instabilities and measurement-dependent behavior.[18−25] These instabilities vary widely between device structures due to different processing methods, such as growth in ambient or in controlled atmospheres, and due to measurement conditions. The origins of this behavior are attributed to a variety of mechanisms including mass diffusion of ions,[25−27] structural changes,[28] and grain boundaries.[29]

While there has been intense effort directed at understanding the optoelectronic performance of organic metal halide materials, there has been less work to understand their properties more broadly as semiconductors. Work by Mitzi and co-workers demonstrated field effect devices in Sn-based compounds with layered structures some years ago.[30] Despite high reported carrier mobilities,[16] easily accessible conduction and valence band energies,[31] and previous reports employing other hybrid perovskites,[30] field-effect transistors (FETs) based on methylammonium lead iodide ((MA)$PbI_3$) have, until very recently,[32] remained notably absent from the literature.

A number of studies have considered the possibility that ionic migration[18,20,25−27,33] or ferroelectric polarization[34−36] are pertinent processes in perovskite solar cells, though substantial debate remains.[37] Ionic migration has been observed in a number of oxide and halide materials adopting the perovskite structure,[38−42] and has recently been studied experimentally

**Received:** August 1, 2015
**Accepted:** August 27, 2015
**Published:** August 31, 2015





DOI: 10.1021/acs.jpclett.5b01669
J. Phys. Chem. Lett. 2015, 6, 3565−3571

and computationally in $(MA)PbI_3$.[26,33] Here we have fabricated a set of electronic devices based on $(MA)PbI_3$ in order to study the nature of electrical instabilities in this system. By measuring the electrical characteristics of FETs, capacitors and solar cells as a function of temperature, we observe behavior consistent with a substantial susceptibility to polarization, potentially due to ionic mass transport within thin films of $(MA)PbI_3$.

To examine the electrical behavior of thin films of $(MA)PbI_3$, we fabricated bottom-gate, top-contact (BGTC) FETs (see inset to Figure 1a). The $(MA)PbI_3$ was deposited using recently reported[12,43] solvent-annealing techniques, as applied to planar-architecture PV cells. A solution of $(MA)PbI_3$ was formed from a 1:1 molar ratio of lead iodide ($PbI_2$) and $CH_3NH_3I$. The solution was deposited via spin-casting in ambient-pressure $N_2$, and chlorobenzene (which does not dissolve $(MA)PbI_3$) was applied to the film during the spin-casting process. More details are provided in the Supporting Information.

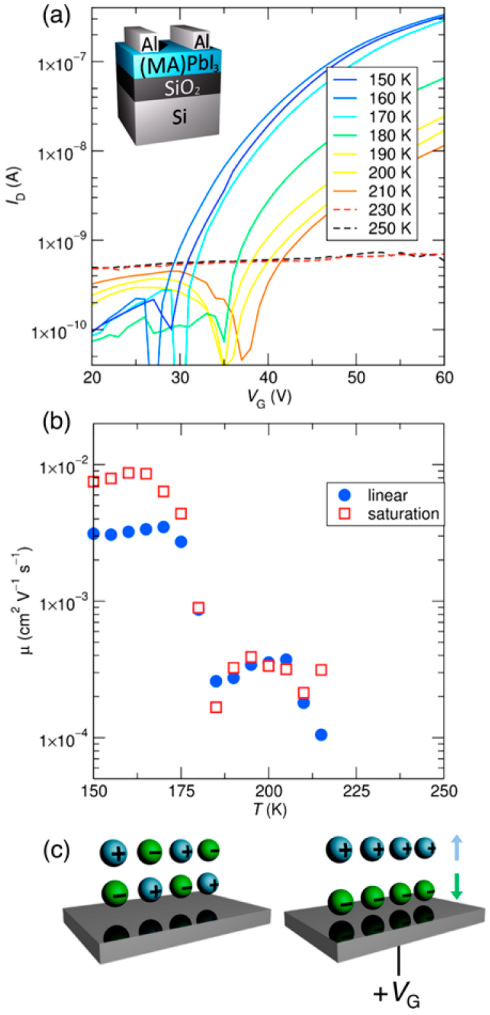


**Figure 1.** (a) Transfer curves (drain current as a function of gate voltage) of methylammonium lead iodide field-effect transistor measured at various temperatures between 150 and 250 K. The device had a length and width of 200 $\mu$m and 2600 $\mu$m, respectively, and the geometric capacitance of the dielectric was 23 nF $cm^{-2}$. Inset: schematic representation of field-effect transistor structure employed in this study. Si labels the silicon gate electrode, $SiO_2$ the 150 nm silicon oxide dielectric, $(MA)PbI_3$ the methylammonium lead iodide semiconductor layer, and Al the aluminum source and drain electrodes. (b) Approximated field-effect mobility evaluated using the gradual-channel approximation as a function of measurement temperature. Above 215 K, the measured drain current was comparable to or less than the gate current and hence mobility values are not plotted for these points. (c) Schematic representation of proposed polarization mechanism of mobile ionic species in methylammonium lead iodide perovskite, under the influence of external applied gate field ($V_G$).

We found that the electrical characteristics of $(MA)PbI_3$ had a complex temperature dependence. At room temperature these devices exhibit low source-drain currents and no field-induced current modulation (see Figure 1a). However, when the temperature is reduced below 220 K, a field-effect is observed and the drain current continues to increase as the temperature is reduced. Where the drain current is observed to be substantially in excess of gate current, the gradual-channel approximation[44] has been applied to extract a value of field-effect mobility. The gradual channel approximation for extraction of carrier mobility in field-effect devices assumes a single electronic charge carrier, uniform carrier accumulation in the channel, and time-independent behavior, and consequently does not provide a simple estimation of the carrier motion for measurements with nonideal effects. This is consistent with our observation of absolute values of electron mobility substantially lower than those previously reported using other techniques.[16] Nonetheless, it can be applied as a proxy for relative transistor performance, assuming a high transconductance is desirable. Since aluminum source and drain electrodes have been employed here, only electron transport is observed. This is as one would expect given the position of the valence band and conduction band energies of $(MA)PbI_3$ relative to the work function of aluminum.[31] As shown in Figure 1b a roughly temperature-independent mobility is observed, with the exception of an approximately 1 order of magnitude change in mobility around 180 K. Above 215 K, the drain current was too low to apply the gradual-channel approximation, and these points have not been plotted.

If $(MA)PbI_3$ exhibits substantial polarization susceptibility (via mobile ions or alignment of the dipolar molecular cation, for example), one would expect the application of an electric field to result in the absorption of energy by the structure, and an electronic screening effect in electronic devices (see Figure 1c).[33] Such a mechanism should be expected to result in a screening of applied gate fields in FETs and hence inhibit accumulation of carriers and the electrical conductivity of the channel. Both the diffusion of ionic species and polarization due to local molecular motion in the solid are expected to be temperature-activated.[33,34,45] For this reason one should expect that over the time-scales relevant for measurement of field-effect conduction (typically 10s of ms to 1s per data point), the screening mechanism can be strongly suppressed by reducing the temperature of the device. The larger aliphatic or aromatic (di)ammonium cations employed in previously reported hybrid halide FETs[30] led to a 2D layered structure rather than the 3D structure of $(MA)PbI_3$. It is likely that these larger cations are less mobile than methylammonium cations, which could consequently lead to a substantially diminished screening effect if this species is indeed responsible for the observed behavior.

These observations are consistent with temperature-dependent dielectric properties or temperature-activated ionic migration. The temperature-independence of mobility below 210 K (aside from the discontinuity in mobility at 180 K) is attributed to two competing effects. Charge transport in polycrystalline and disordered semiconductors is described by


DOI: 10.1021/acs.jpclett.5b01669
J. Phys. Chem. Lett. 2015, 6, 3565−3571

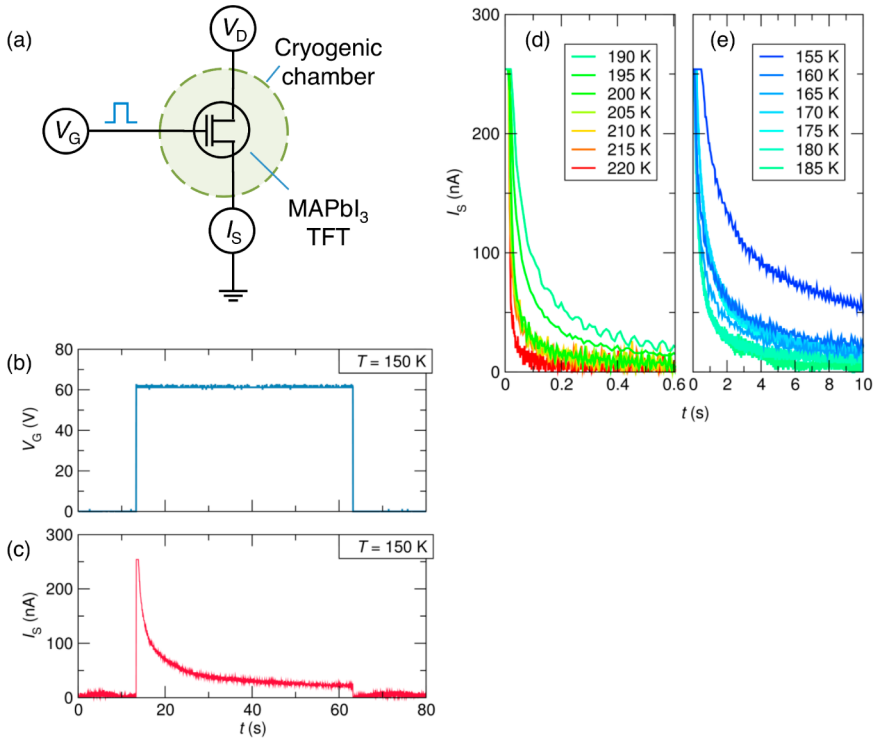


**Figure 2.** (a) Schematic representation of experimental setup for low-temperature, time-dependent field-effect transistor (FET) measurements. A constant voltage ($V_D$) is applied to the drain terminal, a pulsed voltage is applied to the gate terminal ($V_G$), and the source-drain current ($I_{DS}$) is monitored at the source terminal. (b) Gate voltage and (c) source-drain current as a function of time in methylammonium lead iodide FET, measured at 150 K. (d,e) Source-drain current of methylammonium lead iodide FET as a function of time, measured at various temperatures. The device had a length and width of 200 $\mu$m and 2600 $\mu$m, respectively, and the geometric capacitance of the dielectric was 23 nF cm$^{-2}$.

temperature-activated processes[46] and hence one should expect to observe a reduced carrier mobility with lower temperature. However, as described above, over the time-scales relevant for electrical measurements, screening effects are expected to inhibit carrier accumulation in transistor devices and can hence be expected to lead to an increased observed mobility with reducing temperature as the effect of screening is reduced. The convolution of these two phenomena is expected to be complex, and it is hence difficult to make detailed *a priori* predictions on the temperature-dependence of apparent mobility in this system. The reason behind the observed change in mobility between 175 and 185 K is unclear. There exists a known structural phase transition in (MA)PbI$_3$ at a temperature of 163 K.[16,47] The structure is found to change phase from tetragonal ($\beta$) above 163 K to orthorhombic ($\gamma$) below 163 K. The transition temperature was experimentally verified via laboratory powder X-ray diffraction (Figure S3, further details in the Supporting Information). Such a change in unit cell will invariably lead to changes in carrier wave function overlap and hence charge transport properties. The temperature of this structural phase transition is known to be dependent on exposure to $H_2O$.[47] Hence it is not unreasonable to consider the possibility that the change in mobility observed in Figure 1b is due to such a phase transition.

To investigate the time-dependence of potential polarization mechanisms in (MA)PbI$_3$, we carried out a set of pulsed-gate measurements on a FET at various temperatures. Such dynamic measurements have proven useful to study nonidealities in FETs in the past.[48] A device identical to that illustrated in the inset to Figure 1a was measured using the setup illustrated in Figure 2a. The temperature of the device was reduced to 150 K, the drain current was held constant, and a pulsed voltage was applied to the gate electrode (Figure 2b). The source-drain current was then measured as a function of time (Figure 2c). We observe a fast (~5 $\mu$s) rise in source-drain current (due to electronic injection) followed by a much slower decay over several seconds. The latter process is attributed to a slow polarization within the perovskite layer and an accumulation of repulsive ionic charge at the (otherwise neutral) semiconductor-dielectric interface. The capacitive nature of the planar FET architecture is known to limit the frequency response of transistors subjected to oscillatory gate voltages.[49] However, this frequency is expected[49] to be many orders of magnitude higher than those under investigation in Figure 2, and this phenomenon can hence be neglected.

We observed a strong dependence of the source-drain current in FETs as a function of time and temperature. As the temperature of the FET was increased, the decay rate of the current after application of a gate bias increases substantially (see Figure 2d and 2e). This behavior is again compatible with a temperature-dependent polarization process taking place within the structure and explains why it is not possible to measure working transistors at room temperature, at normal measurement speeds. Although a number of polarization mechanisms are possible in this material, one can broadly separate these phenomena into ionic migration (which should occur on the length scale of the film thickness) and atomic or molecular dipole creation or alignment (which occur on an atomic/molecular length scale for dipole creation or microstructural length scale for domain alignment). In an attempt to elucidate the more likely mechanism, we carried out a set of impedance measurements on (MA)PbI$_3$ capacitor structures,


DOI: 10.1021/acs.jpclett.5b01669
J. Phys. Chem. Lett. 2015, 6, 3565−3571

akin to similar recent studies.[18,21,22] The structure studied is shown in the inset to Figure 3a. Relative permittivity was

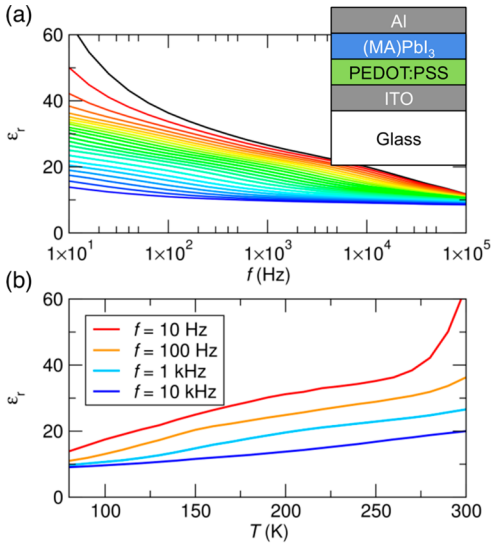


**Figure 3.** (a) Relative permittivity of $(MA)PbI_3$ capacitor, extracted using the two-component circuit model described in the Supporting Information as a function of temperature, at various temperatures between 80 K and 300 K. Device area was 0.042 $cm^2$. Inset: Schematic representation of capacitor structure employed in this study. ITO labels the indium tin oxide bottom-electrode, PEDOT:PSS poly(3,4-ethylenedioxythiophene) polystyrenesulfonate, $(MA)PbI_3$ the methylammonium lead iodide semiconductor layer, and Al the aluminum top electrode. (b) The same data presented as a function of temperature for various frequencies.

extracted from the impedance spectra using a 2-component circuit model as described in the Supporting Information, and is plotted as a function of frequency and temperature in Figure 3a,b. Of note are the strong temperature- and frequency-dependence of the permittivity, and the high value in an absolute sense. The apparent permittivity is somewhat insensitive to the measurement temperature in the high-frequency regime but increases substantially with increasing temperature in the low-frequency regime. This trend is not observed in dielectric measurements of single crystals[50] and is consistent with microstructural effects in these polycrystalline thin films.[51] This behavior can be explained by two phenomena: grain boundary polarization, wherein relatively conductive grains are separated by electronically insulating grain boundaries, and space charge polarization due to ionic migration that is enhanced along grain boundaries. Both mechanisms would exhibit the observed temperature dependence, though long-range ionic diffusion under an applied field would dominate at slower frequencies. Indeed, this hypothesis is consistent with the greater hysteresis observed in $(MA)PbI_3$ films deposited on mesoporous $TiO_2$,[20,52] wherein infiltration of $(MA)PbI_3$ into the nanoscale pores of the $TiO_2$ results in nanocrystalline grains with only local structural coherence.[53] This effectively creates a multitude of pathways for facile ionic migration and a large area of interphase boundaries where interfacial polarization may occur. Although it is difficult to deconvolute the impact of each mechanism that contributes to dielectric relaxation, the general trend suggests that slower phenomena (e.g., proton migration or vacancy-mediated migration of the iodide anion) may be primarily responsible for the observed behavior in FET devices.[33] To ensure that this experiment is an effective probe of the $(MA)PbI_3$ and is not substantially perturbed by relaxation phenomena in the interfacial layers, an identical experiment was carried out on a similar structure with the $(MA)PbI_3$ layer omitted (see Supporting Information Figure S2). Indeed, in this simplified structure, only purely resistive behavior was observed in the frequency range of interest.

As has been suggested recently,[25,33] if one or more ionic species in the $(MA)PbI_3$ structure are mobile, it is not only possible that these could be relevant for device instabilities, but could also conceivably lead to favorable internal electric fields, potentially aiding charge separation and extraction. Here we have investigated how the relative power conversion efficiency of $(MA)PbI_3$ photovoltaic cells change as a function of the measurement temperature. We fabricated $(MA)PbI_3$ photovoltaic cells in a planar architecture (inset to Figure 4a),[54] using

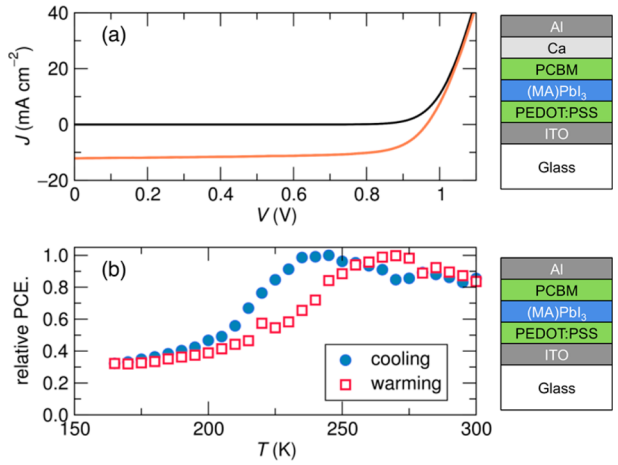


**Figure 4.** (a) Current−voltage characteristics of an example methylammonium lead iodide photovoltaic (PV) cell with calcium/aluminum top electrode, measured in the dark and under 1 sun illumination from AM1.5 solar spectrum, under atmospheric pressure $N_2$. Schematic representation of the PV structure employed in this study is displayed alongside. ITO labels the indium tin oxide bottom-electrode, PEDOT:PSS is poly(3,4-ethylenedioxythiophene) polystyrenesulfonate, $(MA)PbI_3$ is the methylammonium lead iodide semiconductor layer, PCBM is phenyl-$C_{61}$-butyric acid methyl ester, and Ca and Al are the calcium and aluminum top electrodes. (b) Relative power-conversion efficiency of methylammonium lead iodide photovoltaic cell with aluminum top electrode (structure alongside) as a function of temperature, under illumination from monochromatic green (530 nm) light. Device area was 0.06 $cm^2$ in all cases.

the same deposition method as the FETs (see Supporting Information for more detail).[12,43] When measured under atmospheric-pressure $N_2$, the devices exhibited power conversion efficiencies in excess of 9% (see Figure 4a). These values give us confidence that any relative PCE measurements are representative of the device itself, rather than any nonidealities. The thickness of the $MAPbI_3$ film (~100 nm) has not been optimized for PV cells, and one would expect to observe higher power conversion efficiencies for a thicker film. By illuminating the device with green (530 nm) light, which is well within the band gap of the material, we were able to gain insight into how the efficiency of the device evolves with reducing temperature. Green light was chosen, rather than the full solar spectrum, to eliminate any effects of shifts in the band gap with temperature that can influence measurements with


DOI: 10.1021/acs.jpclett.5b01669
J. Phys. Chem. Lett. 2015, 6, 3565−3571

broad band illumination. In order to avoid oxidation, during the brief (~1 m) exposure to air when loading samples into the cryogenic probe station, an aluminum top electrode was employed in this case, rather than a calcium/aluminum electrode, as was the case for the devices measured under $N_2$ (see inset to Figure 4b). As previously reported for a AM1.5 spectrum,[55] we see a significant reduction in the relative power-conversion efficiency of these devices as the operating temperature is reduced. Because a green light source is employed at constant intensity (200 mW/cm$^2$), we have here plotted PCE relative to the maximum value (at 245 K), rather than absolute values. We see that while there is a small amount of hysteresis between reducing temperature and increasing temperature, the behavior is completely reversible. The delay between each temperature was approximately 10 min, and we attribute the hysteresis to a lag between the temperature of the sample and that reported by the thermocouple, due to the thermal conductivity of the substrate. While the short-circuit current ($J_{sc}$) of the device was found to fall to about half its original value when the temperature is reduced from 300 to 160 K, the open-circuit voltage ($V_{oc}$) increased from 0.8 V at 300 K to 0.9 V at 160 K. More details on the evolution of the device parameters are given in the Supporting Information (Section S4), and we consider the major features here. One would typically expect an ideal diode to exhibit a reducing $V_{oc}$ with increasing temperature,[56] as observed here. The decrease in $J_{sc}$ as the temperature is lowered is unlikely due to a reduction in charge generation with temperature, therefore it is likely a result of recombination before charge extraction. Whether there are specific trap sites in the bulk or whether it is related to the contacts to the cell, the effects show the largest change at the temperature where we see dramatic changes in the behavior of the FETs. This observation is consistent with our suggestion that mass-transport in the $(MA)PbI_3$ may not only be (at least partially) responsible for the observed instabilities in electronic devices based upon this system, but could be a contributor to the high performance of photovoltaic cells.

In summary, we have presented results from temperature-dependent measurements of $(MA)PbI_3$ electronic devices that, when viewed collectively, suggest the existence of a substantial susceptibility to polarization at temporal and spatial scales that significantly impact the electrical behavior of the material. Many questions remain, including the details of the mechanism, or mechanisms, responsible for the observed behavior, and whether and how these polarization phenomena may be advantageously suppressed (or enhanced) to improve the performance of $(MA)PbI_3$ thin films. Similarly, if ionic migration is responsible, it is unclear as to which species are mobile, and whether it is interstitial species or vacancy defects that are responsible for the observed behavior.[22] Our work suggests that measurements of multiple types of device structures can be useful in understanding the properties and behavior of $(MA)PbI_3$, and that future work on transport in field-effect devices is a fruitful complement to that on solar cells.

## ■ ASSOCIATED CONTENT

### Supporting Information

Supporting Information contains details of methylammonium iodide synthesis, methylammonium lead iodide ($(MA)PbI_3$) thin-film preparation, field-effect transistor fabrication and measurement, capacitor fabrication and measurement, photovoltaic cell fabrication and measurement, an analysis of $(MA)PbI_3$ capacitor impedance spectra, an analysis of poly(3,4-ethylenedioxythiophene) polystyrenesulfonate capacitor impedance spectra and temperature-dependent powder X-ray diffraction of polycrystalline $(MA)PbI_3$. The Supporting Information is available free of charge on the ACS Publications website at DOI: 10.1021/acs.jpclett.5b01669.

(PDF)

## ■ AUTHOR INFORMATION

### Corresponding Author

*Address: Materials Department, University of California, Santa Barbara CA 93106-5050. E-mail: mchabinyc@engineering.ucsb.edu.

### Notes

The authors declare no competing financial interest.

## ■ ACKNOWLEDGMENTS

This work was supported by the U.S. Department of Energy, Office of Science, Basic Energy Sciences under award number DE-SC-0012541. The UCSB-U Texas El Paso collaboration was supported by the NSF PREM award DMR-1205302. Partial support of the research was provided by the MC-CAM Program at UCSB sponsored by Mitsubishi Chemical Corporation (Japan). Use of the shared experimental facilities of the Materials Research Laboratory at UCSB was supported by the MRSEC Program of the National Science Foundation under Award No. DMR 1121053. J.G.L. gratefully acknowledges Virgil Elings and Betty Elings Wells for financial support through the Elings Fellowship Awards. A.J.L. gratefully acknowledges support of Swiss National Science Foundation fellowship number PBSKP2-145825.

## ■ REFERENCES

(1) Carlson, D. E.; Wronski, C. R. Amorphous Silicon Solar Cell. *Appl. Phys. Lett.* **1976**, *28*, 671−673.
(2) Tang, C. W. Two-Layer Organic Photovoltaic Cell. *Appl. Phys. Lett.* **1986**, *48*, 183−185.
(3) Sariciftci, N. S.; Smilowitz, L.; Heeger, A. J.; Wudl, F. Photoinduced Electron Transfer from a Conducting Polymer to Buckminsterfullerene. *Science* **1992**, *258*, 1474−1476.
(4) O'Regan, B.; Gratzel, M. A Low-Cost, High-Efficiency Solar Cell Based on Dye-Sensitized Colloidal $TiO_2$ Films. *Nature* **1991**, *353*, 737−740.
(5) Britt, J.; Ferekides, C. Thin-film CdS/CdTe Solar Cell with 15.8% Efficiency. *Appl. Phys. Lett.* **1993**, *62*, 2851−2852.
(6) Kojima, A.; Teshima, K.; Shirai, Y.; Miyasaka, T. Organometal Halide Perovskites as Visible-Light Sensitizers for Photovoltaic Cells. *J. Am. Chem. Soc.* **2009**, *131*, 6050−6051.
(7) Lee, P. A.; Nagaosa, N.; Wen, X.-G. Doping a Mott insulator: Physics of High-Temperature Superconductivity. *Rev. Mod. Phys.* **2006**, *78*, 17−85.
(8) Johnston, D. C. The Puzzle of High Temperature Superconductivity in Layered Iron Pnictides and Chalcogenides. *Adv. Phys.* **2010**, *59*, 803−1061.
(9) Lee, M. M.; Teuscher, J.; Miyasaka, T.; Murakami, T. N.; Snaith, H. J. Efficient Hybrid Solar Cells Based on Meso-Superstructured Organometal Halide Perovskites. *Science* **2012**, *338*, 643−647.
(10) Gratzel, M. The Light and Shade of Perovskite Solar Cells. *Nat. Mater.* **2014**, *13*, 838−842.
(11) Zhou, H.; Chen, Q.; Li, G.; Luo, S.; Song, T.-b.; Duan, H.-S.; Hong, Z.; You, J.; Liu, Y.; Yang, Y. Interface Engineering of Highly Efficient Perovskite Solar Cells. *Science* **2014**, *345*, 542−546.
(12) Jeon, N. J.; Noh, J. H.; Kim, Y. C.; Yang, W. S.; Ryu, S.; Seok, S. I. Solvent Engineering for High-Performance Inorganic−Organic Hybrid Perovskite Solar Cells. *Nat. Mater.* **2014**, *13*, 897−903.



DOI: 10.1021/acs.jpclett.5b01669
*J. Phys. Chem. Lett.* 2015, 6, 3565−3571

(13) Yang, W. S.; Noh, J. H.; Jeon, N. J.; Kim, Y. C.; Ryu, S.; Seo, J.; Seok, S. I. High-Performance Photovoltaic Perovskite Layers Fabricated Through Intramolecular Exchange. *Science* **2015**, *348*, 1234−1237.
(14) You, J.; Hong, Z.; Yang, Y.; Chen, Q.; Cai, M.; Song, T.-B.; Chen, C.-C.; Lu, S.; Liu, Y.; Zhou, H.; et al. Low-Temperature Solution-Processed Perovskite Solar Cells with High Efficiency and Flexibility. *ACS Nano* **2014**, *8*, 1674−1680.
(15) Papavassiliou, G. C.; Koutselas, I. B. Structural, Optical and Related Properties of Some Natural Three- and Lower-Dimensional Semiconductor Systems. *Synth. Met.* **1995**, *71*, 1713−1714.
(16) Stoumpos, C. C.; Malliakas, C. D.; Kanatzidis, M. G. Semiconducting Tin and Lead Iodide Perovskites with Organic Cations: Phase Transitions, High Mobilities, and Near-Infrared Photoluminescent Properties. *Inorg. Chem.* **2013**, *52*, 9019−9038.
(17) De Wolf, S.; Holovsky, J.; Moon, S.-J.; Löper, P.; Niesen, B.; Ledinsky, M.; Haug, F.-J.; Yum, J.-H.; Ballif, C. Organometallic Halide Perovskites: Sharp Optical Absorption Edge and Its Relation to Photovoltaic Performance. *J. Phys. Chem. Lett.* **2014**, *5*, 1035−1039.
(18) Dualeh, A.; Moehl, T.; Tétreault, N.; Teuscher, J.; Gao, P.; Nazeeruddin, M. K.; Grätzel, M. Impedance Spectroscopic Analysis of Lead Iodide Perovskite-Sensitized Solid-State Solar Cells. *ACS Nano* **2014**, *8*, 362−373.
(19) Snaith, H. J.; Abate, A.; Ball, J. M.; Eperon, G. E.; Leijtens, T.; Noel, N. K.; Stranks, S. D.; Wang, J. T.-W.; Wojciechowski, K.; Zhang, W. Anomalous Hysteresis in Perovskite Solar Cells. *J. Phys. Chem. Lett.* **2014**, *5*, 1511−1515.
(20) Unger, E. L.; Hoke, E. T.; Bailie, C. D.; Nguyen, W. H.; Bowring, A. R.; Heumuller, T.; Christoforo, M. G.; McGehee, M. D. Hysteresis and Transient Behavior in Current-Voltage Measurements of Hybrid-Perovskite Absorber Solar Cells. *Energy Environ. Sci.* **2014**, *7*, 3690−3698.
(21) Almora, O.; Zarazua, I.; Mas-Marza, E.; Mora-Sero, I.; Bisquert, J.; Garcia-Belmonte, G. Capacitive Dark Currents, Hysteresis, and Electrode Polarization in Lead Halide Perovskite Solar Cells. *J. Phys. Chem. Lett.* **2015**, *6*, 1645−1652.
(22) Heo, J. H.; Song, D. H.; Han, H. J.; Kim, S. Y.; Kim, J. H.; Kim, D.; Shin, H. W.; Ahn, T. K.; Wolf, C.; Lee, T.-W.; Im, S. H. Planar $CH_3NH_3PbI_3$ Perovskite Solar Cells with Constant 17.2% Average Power Conversion Efficiency Irrespective of the Scan Rate. *Adv. Mater.* **2015**, *27*, 3424−3430.
(23) Ono, L. K.; Raga, S. R.; Wang, S.; Kato, Y.; Qi, Y. Temperature-dependent hysteresis effects in perovskite-based solar cells. *J. Mater. Chem. A* **2015**, *3*, 9074−9080.
(24) Xiao, Z.; Yuan, Y.; Shao, Y.; Wang, Q.; Dong, Q.; Bi, C.; Sharma, P.; Gruverman, A.; Huang, J. Giant Switchable Photovoltaic Effect in Organometal Trihalide Perovskite Devices. *Nat. Mater.* **2015**, *14*, 193−198.
(25) Zhang, Y.; Liu, M.; Eperon, G. E.; Leijtens, T. C.; McMeekin, D.; Saliba, M.; Zhang, W.; de Bastiani, M.; Petrozza, A.; Herz, L. M.; Johnston, M. B.; Lin, H.; Snaith, H. J. Charge Selective Contacts, Mobile Ions and Anomalous Hysteresis in Organic-Inorganic Perovskite Solar Cells. *Mater. Horiz.* **2015**, *2*, 315−322.
(26) Yang, T.-Y.; Gregori, G.; Pellet, N.; Grätzel, M.; Maier, J. The Significance of Ion Conduction in a Hybrid Organic−Inorganic Lead-Iodide-Based Perovskite Photosensitizer. *Angew. Chem., Int. Ed.* **2015**, *54*, 7905−7910.
(27) Tress, W.; Marinova, N.; Moehl, T.; Zakeeruddin, S. M.; Nazeeruddin, M. K.; Gratzel, M. Understanding the rate-dependent J-V hysteresis, slow time component, and aging in $CH_3NH_3PbI_3$ Perovskite Solar Cells: The Role of a Compensated Electric Field. *Energy Environ. Sci.* **2015**, *8*, 995−1004.
(28) Niu, G.; Guo, X.; Wang, L. Review of Recent Progress in Chemical Stability of Perovskite Solar Cells. *J. Mater. Chem. A* **2015**, *3*, 8970−8980.
(29) Nie, W.; Tsai, H.; Asadpour, R.; Blancon, J.-C.; Neukirch, A. J.; Gupta, G.; Crochet, J. J.; Chhowalla, M.; Tretiak, S.; Alam, M. A.; Wang, H.-L.; Mohite, A. D. High-Efficiency Solution-Processed Perovskite Solar Cells with Millimeter-Scale Grains. *Science* **2015**, *347*, 522−525.
(30) Kagan, C. R.; Mitzi, D. B.; Dimitrakopoulos, C. D. Organic-Inorganic Hybrid Materials as Semiconducting Channels in Thin-Film Field-Effect Transistors. *Science* **1999**, *286*, 945−947.
(31) Kim, H.-S.; Lee, C.-R.; Im, J.-H.; Lee, K.-B.; Moehl, T.; Marchioro, A.; Moon, S.-J.; Humphry-Baker, R.; Yum, J.-H.; Moser, J. E.; Gratzel, M.; Park, N.-G. Lead Iodide Perovskite Sensitized All-Solid-State Submicron Thin Film Mesoscopic Solar Cell with Efficiency Exceeding 9%. *Sci. Rep.* **2012**, *2*, 591.
(32) Mei, Y.; Zhang, C.; Vardeny, Z. V.; Jurchescu, O. D. Electrostatic Gating of Hybrid Halide Perovskite Field-Effect Transistors: Balanced Ambipolar Transport at Room-Temperature. *MRS Commun.* **2015**, *5*, 297−301.
(33) Eames, C.; Frost, J. M.; Barnes, P. R. F.; O'Regan, B. C.; Walsh, A.; Islam, M. S. Ionic Transport in Hybrid Lead Iodide Perovskite Solar Cells. *Nat. Commun.* **2015**, *6*, 7497.
(34) Frost, J. M.; Butler, K. T.; Brivio, F.; Hendon, C. H.; van Schilfgaarde, M.; Walsh, A. Atomistic Origins of High-Performance in Hybrid Halide Perovskite Solar Cells. *Nano Lett.* **2014**, *14*, 2584−2590.
(35) Frost, J. M.; Butler, K. T.; Walsh, A. Molecular Ferroelectric Contributions to Anomalous Hysteresis in Hybrid Perovskite Solar Cells. *APL Mater.* **2014**, *2*, 081506.
(36) Leguy, A. M. A.; Frost, J. M.; McMahon, A. P.; Sakai, V. G.; Kockelmann, W.; Law, C.; Li, X.; Foglia, F.; Walsh, A.; O'Regan, B. C.; Nelson, J.; Cabral, J. T.; Barnes, P. R. F. The Dynamics of Methylammonium Ions in Hybrid Organic-Inorganic Perovskite Solar Cells. *Nat. Commun.* **2015**, *6*, 7780.
(37) Beilsten-Edmands, J.; Eperon, G. E.; Johnson, R. D.; Snaith, H. J.; Radaelli, P. G. Non-Ferroelectric Nature of the Conductance Hysteresis in $CH_3NH_3PbI_3$ Perovskite-Based Photovoltaic Devices. *Appl. Phys. Lett.* **2015**, *106*, 173502.
(38) Mizusaki, J.; Arai, K.; Fueki, K. Ionic Conduction of the Perovskite-Type Halides. *Solid State Ionics* **1983**, *11*, 203−211.
(39) Ishigaki, T.; Yamauchi, S.; Kishio, K.; Mizusaki, J.; Fueki, K. Diffusion of Oxide Ion Vacancies in Perovskite-Type Oxides. *J. Solid State Chem.* **1988**, *73*, 179−187.
(40) Iwahara, H. Oxide-Ionic and Protonic Conductors Based on Perovskite-Type Oxides and Their Possible Applications. *Solid State Ionics* **1992**, *52*, 99−104.
(41) Inaguma, Y.; Liquan, C.; Itoh, M.; Nakamura, T.; Uchida, T.; Ikuta, H.; Wakihara, M. High Ionic Conductivity in Lithium Lanthanum Titanate. *Solid State Commun.* **1993**, *86*, 689−693.
(42) Kawakami, Y.; Fukuda, M.; Ikuta, H.; Wakihara, M. Ionic Conduction of Lithium for Perovskite Type Compounds, $(Li_{0.05}La_{0.317})_{1-x}Sr_{0.5x}NbO_3$, $(Li_{0.1}La_{0.3})_{1-x}Sr_{0.5x}NbO_3$ and $(Li_{0.25}La_{0.25})_{1-x}M_{0.5x}NbO_3$ (M = Ca and Sr). *Solid State Ionics* **1998**, *110*, 187−192.
(43) Jung, J. W.; Williams, S. T.; Jen, A. K. Y. Low-Temperature Processed High-Performance Flexible Perovskite Solar Cells via Rationally Optimized Solvent Washing Treatments. *RSC Adv.* **2014**, *4*, 62971−62977.
(44) Sze, S. M.; Ng, K. K. *Physics of Semiconductor Devices*; Wiley: New York, 2006.
(45) Bazant, M. Z.; Thornton, K.; Ajdari, A. Diffuse-charge dynamics in electrochemical systems. *Phys. Rev. E* **2004**, *70*, 021506.
(46) Vissenberg, M. C. J. M.; Matters, M. Theory of The Field-Effect Mobility in Amorphous Organic Transistors. *Phys. Rev. B: Condens. Matter Mater. Phys.* **1998**, *57*, 12964−12967.
(47) Baikie, T.; Fang, Y.; Kadro, J. M.; Schreyer, M.; Wei, F.; Mhaisalkar, S. G.; Graetzel, M.; White, T. J. Synthesis and Crystal Chemistry of the Hybrid perovskite $(CH_3NH_3)PbI_3$ for Solid-State Sensitised Solar Cell Applications. *J. Mater. Chem. A* **2013**, *1*, 5628−5641.
(48) Salleo, A.; Endicott, F.; Street, R. A. Reversible and Irreversible Trapping at Room Temperature in Poly(thiophene) Thin-Film Transistors. *Appl. Phys. Lett.* **2005**, *86*, 263505.


DOI: 10.1021/acs.jpclett.5b01669
*J. Phys. Chem. Lett.* 2015, 6, 3565−3571

(49) Jung, K.-D.; Lee, C. A.; Par, D.-W.; Park, B.-G.; Shin, H.; Lee, J. D. Admittance Measurements on OFET Channel and Its Modeling With R-C Network. *IEEE Electron Device Lett.* **2007**, *28*, 204−206.
(50) Onoda-Yamamuro, N.; Matsuo, T.; Suga, H. Dielectric Study of $CH_3NH_3PbX_3$ (X = Cl, Br, I). *J. Phys. Chem. Solids* **1992**, *53*, 935−939.
(51) Almond, D. P.; Bowen, C. R. An Explanation of the Photoinduced Giant Dielectric Constant of Lead Halide Perovskite Solar Cells. *J. Phys. Chem. Lett.* **2015**, *6*, 1736−1740.
(52) Heo, J. H.; Han, H. J.; Kim, D.; Ahn, T. K.; Im, S. H. Hysteresis-Less Inverted $CH_3NH_3PbI_3$ Planar Perovskite Hybrid Solar Cells with 18.1% Power Conversion Efficiency. *Energy Environ. Sci.* **2015**, *8*, 1602−1608.
(53) Choi, J. J.; Yang, X.; Norman, Z. M.; Billinge, S. J. L.; Owen, J. S. Structure of Methylammonium Lead Iodide Within Mesoporous Titanium Dioxide: Active Material in High-Performance Perovskite Solar Cells. *Nano Lett.* **2014**, *14*, 127−133.
(54) Malinkiewicz, O.; Yella, A.; Lee, Y. H.; Espallargas, G. M.; Graetzel, M.; Nazeeruddin, M. K.; Bolink, H. J. Perovskite Solar Cells Employing Organic Charge-Transport Layers. *Nat. Photonics* **2014**, *8*, 128−132.
(55) Zhang, H.; Qiao, X.; Shen, Y.; Moehl, T.; Zakeeruddin, S. M.; Gratzel, M.; Wang, M. Photovoltaic Behaviour of Lead Methylammonium Triiodide Perovskite Solar Cells Down to 80 K. *J. Mater. Chem. A* **2015**, *3*, 11762−11767.
(56) Nelson, J. *The Physics of Solar Cells*; Imperial College Press: London, 2003.



DOI: 10.1021/acs.jpclett.5b01669
*J. Phys. Chem. Lett.* 2015, 6, 3565−3571